npj | science of food

Article

Published in partnership with Beijing Technology and Business University & International Union of Food Science and Technology

https://doi.org/10.1038/s41538-025-00409-8

Abrogating the adenine methylation ability of *Lacticaseibacillus paracasei* improves its freeze-drying and storage resistance

Hui Qiao[1,2,3,4], Mingkun You[1,2,3,4], Jiaming Yan[1,2,3], Meng Zhang[1,2,3], Kwok Lai-Yu[1,2,3] & Wenyi Zhang[1,2,3] ✉

Freeze-drying is a widely adopted method for the long-term storage of starter cultures in the food industry but can cause cell instability and a decline in post-storage viability. We used an unmethylated *Lacticaseibacillus paracasei* Zhang mutant lacking adenine-specific DNA-methyltransferase. This mutant was subjected to freeze-drying and stored at 30 °C for two distinct durations (30 and 60 days), Our analysis revealed the unmethylated mutant outperformed the wild-type in cell viability and survival following freeze-drying and post-freeze-drying storage. And significant metabolic pathway differences between the stored mutant and wild-type bacteria. These differences were evident in the phosphotransferase system, carbohydrate, and amino acid metabolism, and fatty acid biosynthesis, and were consistent across transcriptomic, proteomic, and metabolomic analyses. This is achieved by modulating key metabolic pathways within the bacteria. This study contributes to the limited literature on the role of bacterial adenine methylation in industrial strain application and starter culture storage.

Starter cultures are microbial preparations that contain a high density of one or more microorganisms, designed to accelerate or guide the fermentation process for fermented food production[1]. Lyophilization, or freeze-drying, is a common and cost-effective method for preparing these cultures[2]. However, this process subjects cells to physical stresses due to crystal formation, dehydration, and osmotic changes[3], which can lead to protein denaturation and reduced cell viability[4,5]. The stability of starter cultures often declines over extended storage periods, with the cell membrane being particularly susceptible to damage, depending on its physical properties and lipid organization[6]. Numerous strategies have been employed to enhance the viability of probiotics, including improved encapsulation techniques, protective additives, and optimized processing and storage conditions[7]. However, research on epigenetic modifications to improve starter culture storage characteristics is limited. This study explores the novel concept of using DNA methylation to regulate the survival of a lactic acid bacterium starter culture following freeze-drying and storage.

Lacticaseibacillus paracasei (*L. paracasei*) species, known for their probiotic properties, are widely used in commercial products and as dairy starter cultures[8,9]. *Lacticaseibacillus paracasei* Zhang (*L. paracasei* Zhang), a well-studied probiotic strain originated from koumiss, has demonstrated tolerance to acidic environments, bile salts, and simulated gastrointestinal conditions[10,11]. Its genome sequencing and functional genomics have provided insights into its genetics and functional mechanism[12]. DNA methylation is catalyzed by DNA methyltransferases. The process entails the transfer of a methyl group from S-adenosylmethionine to cytosine residues located in CpG dinucleotides within the genome[13]. This modification is a universal epigenetic modification[14], encompassing 4-methylcytosine, 5-methylcytosine, and 6-methyladenine. DNA methylation transmits genetic information and regulates metabolic networks by modulating gene expression. It is a relatively stable modification and can be inherited by progeny during DNA replication without altering the underlying DNA sequence[15]. In bacteria, DNA methyltransferases and epigenetic regulation are crucial for mediating stress responses[16]. Notably, N6-methyladenine (m6A) modification is predominantly found in prokaryotes and protists, and it is also prevalent in approximately 25% of mammalian mRNAs at the same nitrogen position[17]. In prokaryotes, prokaryotic cells use m6A to replicate, repair, transpose, and transcribe DNA[18]. An adenine-specific DNA-methyltransferase, *pglX*, was identified in the genome of *L. paracasei* Zhang using single-molecule real-time sequencing[19]. Inactivating the *pglX* gene in *L. paracasei* Zhang resulted in the creation of a 6-methyladenine methylation-deficient mutant strain, Δ*pglX*[20,21].

Despite its significance, there has been little research on the role of adenine methylation in industrial lactic acid bacteria. The commercial use of these bacteria as food starter cultures hinges on their viability. Freeze-drying

[1]Key Laboratory of Dairy Biotechnology and Engineering, Ministry of Education, Inner Mongolia Agricultural University, Hohhot, People's Republic of China. [2]Key Laboratory of Dairy Products Processing, Ministry of Agriculture, Inner Mongolia Agricultural University, Hohhot, People's Republic of China. [3]Inner Mongolia Key Laboratory of Dairy Biotechnology and Engineering, Inner Mongolia Agricultural University, Hohhot, People's Republic of China. [4]These authors contributed equally: Hui Qiao, Mingkun You. ✉e-mail: zhangwenyizi@163.com

is a widely used method for large-scale starter culture preparation due to its convenience for transport and storage[22]; however, it poses significant stress on the cells, presenting challenges for the food industry in maintaining high bacterial viability and stable freeze-dried stocks for long-term storage[23]. Provided the critical role of DNA methyltransferases and epigenetic regulation in bacterial stress responses[24], this study hypothesized that the methylation state of *L. paracasei* Zhang would influence its viability during freeze-drying and subsequent storage. To test this hypothesis, we compared the viability, transcriptomes, proteomes, and metabolomes of wild-type *L. paracasei* Zhang and the Δ*pglX* mutant after 30 and 60 days of post-freeze-drying storage.

Results

Viability and survival rates of mutant and wild-type strains during storage

The viability of both mutant and wild-type strains decreased over time during storage at 30°C (Fig. 1A). However, the mutant strain consistently maintained a significantly higher viable count compared to the wild-type strain at both assessed time points ($p < 0.05$). The difference in viable counts between the strains also decreased as the storage period extended, with the larger difference observed on day 30 (the viable count difference on day 30: $8.98 \pm 3.08 \times 10^{10}$ CFU/mL; day 60: $5.70 \pm 0.38 \times 10^{10}$ CFU/mL). On the other hand, the survival rates for both strains declined over the storage period (Fig. 1B), with the mutant exhibiting significantly higher survival rates compared to the wild-type strain on both day 30 (34.99% vs 13.88%) and day 60 (23.90% vs 11.23%; $p < 0.05$). Notably, the mutant strain had a higher survival rate after 60 days of storage at 23.90% than the wild-type strain at 13.88% after 30 days.

Differential gene expression of freeze-dried cells over storage durations

To gain a thorough understanding of how storage duration affects gene expression in freeze-dried cells, we compared the gene expression profiles of the mutant and wild-type strains after 30 and 60 days of storage. Differentially expressed genes were identified using a $\log_2$ Fold Change (FC) threshold of ≥ 1 for upregulation and ≤ -1 for downregulation, with an FDR of < 0.05 for statistical significance (Fig. 2A). After 30 days of storage, a total of 215 differentially expressed genes (DEGs) were identified, with 83 upregulated and 132 downregulated. After 60 days, 143 DEGs were identified, with 70 upregulated and 73 downregulated. A subset of 114 DEGs exhibited consistent trends across both time points, with 55 upregulated and 59 downregulated.

Functional annotation and enrichment analysis of DEGs in the mutant Δ*pglX* strain

Functional annotation and enrichment analysis of the DEGs were conducted using the Kyoto Encyclopedia of Genes and Genomes (KEGG) database. The DEGs identified on days 30 and 60 were primarily associated with six first level-KEGG pathway categories: metabolism, genetic information processing, environmental information processing, cellular processes, organismal systems, and human diseases. In the mutant, the DEGs showed a decreasing trend post-storage, predominantly related to membrane transport and carbohydrate metabolism. A small number of DEGs in the mutant increased, primarily related to the metabolism of lipids, amino acids, carbohydrates, energy, and cofactors and vitamins.

Results from the KEGG enrichment analysis (Fig. S1) revealed an enrichment of various pathways after different storage durations, with two pathways enriched on day 30 (fatty acid biosynthesis and phosphotransferase system, PTS) and six pathways on day 60 (PTS, fatty acid biosynthesis, propanoate metabolism, pyruvate metabolism, biofilm formation—*Escherichia coli*, and insulin resistance). Notably, the pathways for fatty acid biosynthesis and PTS were consistently enriched in the mutant strain at both storage time points.

Differential protein expression in freeze-dried cells over storage durations

A comparative analysis of protein expression between the mutant and wild-type strains stored for 30 and 60 days revealed distinct protein expression patterns, based on the cut-off levels of FC ≥ 1.5 or ≤ 0.67 and $p < 0.05$. On days 30 and 60, the number of differentially expressed proteins (DEPs) between the mutant and wild-type strains was 243 (191 increased, 52 decreased) and 234 (185 increased, 49 decreased), respectively (Fig. 2B-C). A large number of DEPs were common to both time points (180 increased, 47 decreased).

Functional annotation and KEGG pathway enrichment of DEPs in the mutant Δ*pglX* strain

The DEPs were functionally annotated using the Gene Ontology (GO) and KEGG databases. The GO categories include biological process, cellular component, and molecular function. Figure S2 illustrates the secondary classification of time point-specific DEPs, which encompasses various categories: under biological processes, there were metabolic process, localization, cellular process, biological regulation, and response to stimulus; under cellular components, there were cellular anatomical entity and protein-containing complex; and under molecular functions, the categories included catalytic activity, binding, transporter activity, transcription regulator activity, antioxidant activity, translation regulator activity, and molecular transducer activity.

Our KEGG annotation found that DEPs were mainly distributed across five first-level KEGG pathway categories, including: metabolism, genetic information processing, environmental information processing, cellular processes, and human diseases.

At the secondary category level, most DEGs belonged to amino acid metabolism, nucleotide metabolism, membrane transport, and carbohydrate metabolism. Furthermore, the KEGG pathway enrichment analysis on DEGs revealed consistent trends of expression at the two storage time

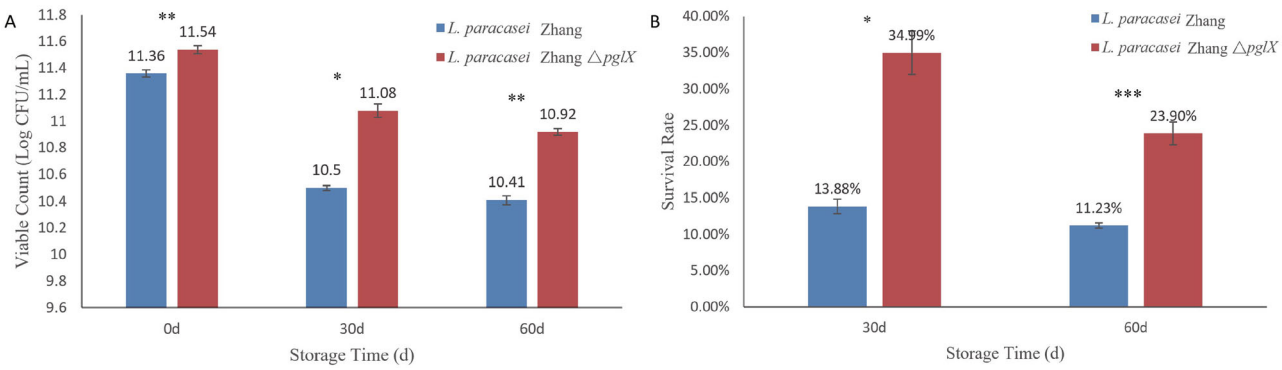

Fig. 1 | Viable counts and survival rates of *L. paracasei Zhang* (wild-type) and *L. paracasei Zhang* ΔpglX (mutant) during storage at 30 °C. Viable counts (**A**) and survival rates (**B**) of *L. paracasei* Zhang (wild-type) and *L. paracasei* Zhang Δ*pglX* (mutant) during storage at 30 °C. Error bars represent standard deviations. Significant differences between the two strains at each time point were evaluated using Student's *t*-tests (* $p < 0.05$; ** $p < 0.01$; *** $p < 0.001$).

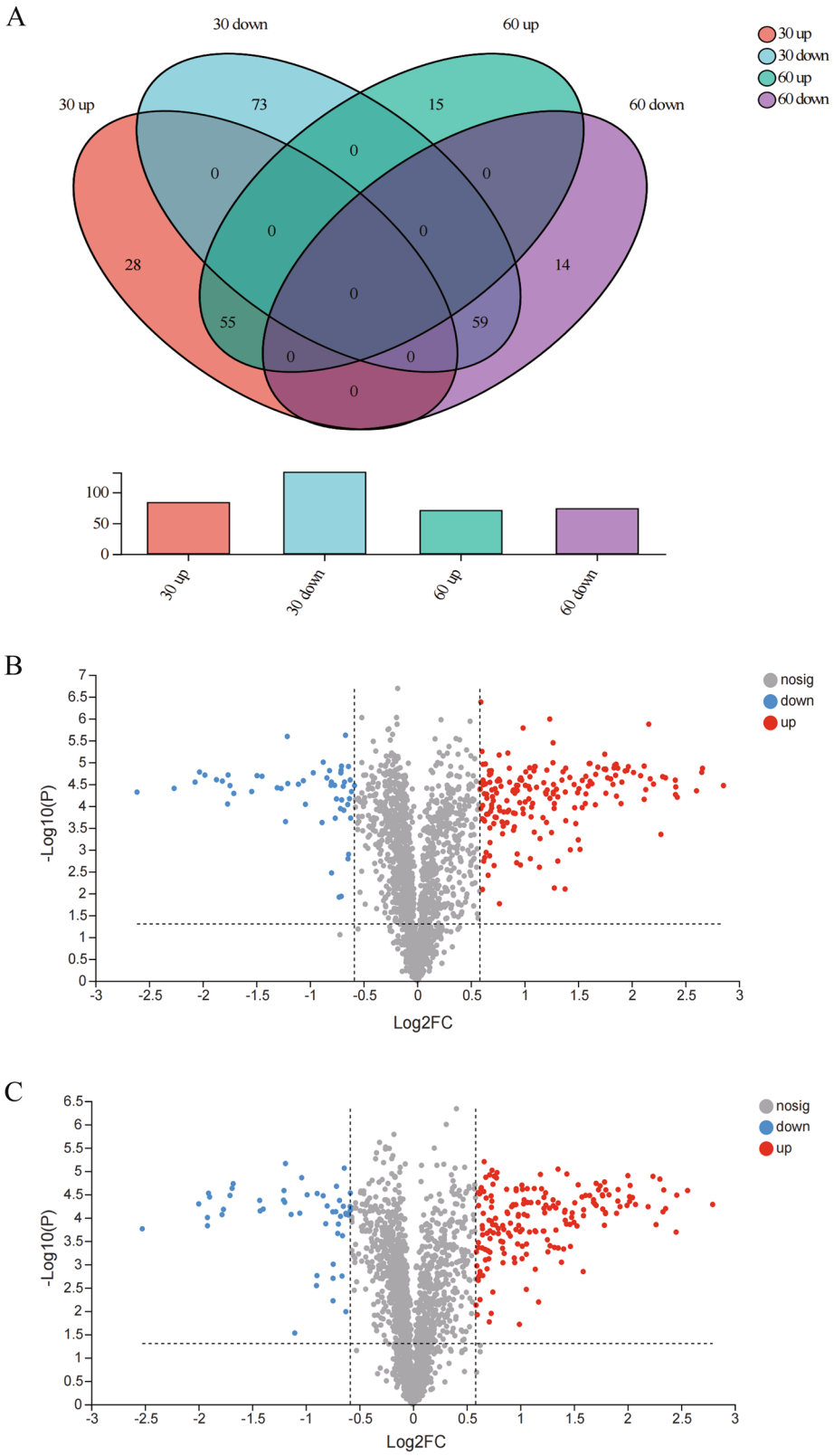

Fig. 2 | The number of differentially expressed genes (DEGs) and differentially expressed proteins (DEPs) between *L. paracasei* Zhang ΔpglX (mutant) and wild-type freeze-dried cells stored for 30 and 60 days. Venn diagram and histogram (**A**) show the number of DEGs in freeze-dried cells stored for 30 and 60 days. Gene sets of up- and down-regulated DEGs after 30 or 60 days of storage are represented as "30 up", "30 down", "60 up", and "60 down", respectively. Volcano plots of DEPs between the mutant and wild-type after (**B**) 30 days and (**C**) 60 days of storage are presented. The x- and y-axes show the fold change and *p*-value of the comparison between the two cell lines, respectively. Each dot in the figure represents a specific protein; grey, blue, and red dots represent non-significant, significantly upregulated, and down-regulated DEPs, respectively (cut-off level: $|FC| \geq 1.5$; $p \leq 0.05$). The number of non-significant, significantly up- regulated, and down-regulated DEPs is indicated in the suffix of the label.

points. Seventeen significantly enriched metabolic pathways were identified (FDR < 0.05; Fig. 3A), with 15 belonging to the first-level KEGG category of metabolism, namely fructose and mannose metabolism, starch and sucrose metabolism, and ascorbate and aldarate metabolism. The two remaining pathways were related to environmental information processing (PTS) and cellular processes (biofilm formation—*Escherichia coli*).

Parallel reaction monitoring (PRM) validation of proteomics results

The precision of proteomics results was validated using PRM protein analysis on 14 selected DEPs. A strong Pearson correlation was found between the two sets of results (day 30: $R = 0.87$, $P = 4.8e\text{-}05$; day 60: $R = 0.9$, $P = 1.1e\text{-}05$), confirming the reliability of the proteomics data (Fig. 3B-C).

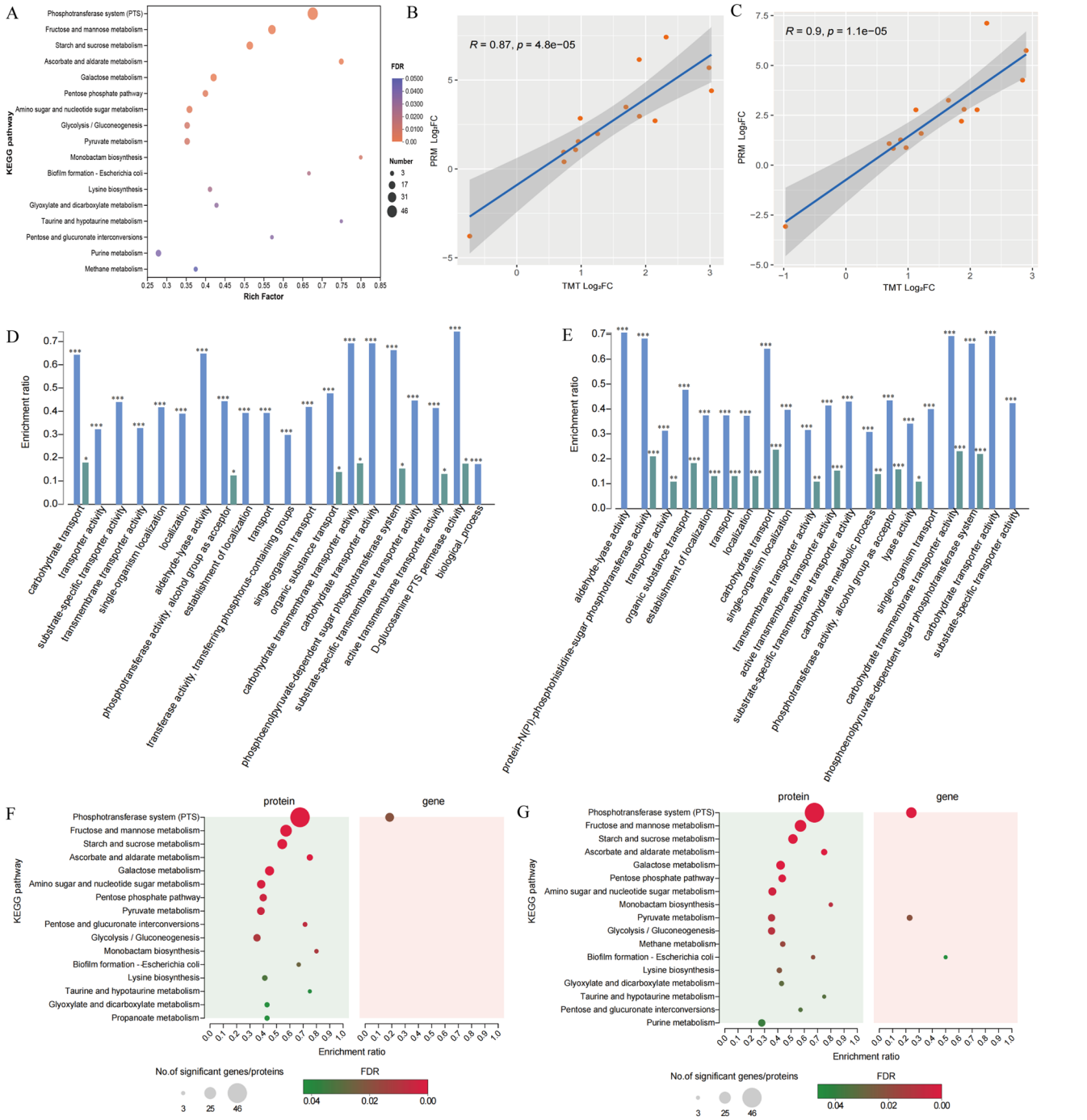

Fig. 3 | Transcriptomic and proteomic analysis results obtained at two storage time points (30 and 60 days). A Kyoto Encyclopedia of Gene and Genomes (KEGG) enrichment analysis of common differentially expressed proteins (DEPs) identified at the two storage time points. The color scale represents the false discovery rate (FDR). Each circle represents a KEGG pathway, with the size of the circle indicating the number of enriched proteins in that specific KEGG pathway. **B**, **C** Scatter plots of Pearson correlation between fold changes identified by tandem mass tag (TMT) labeling and parallel reaction monitoring (PRM) after storing the freeze-dried cells for (**B**) 30 days and (**C**) 60 days. The correlation strength and statistical significance between fold changes found by TMT and PRM are represented by *R* and *p* values, respectively. The grey area shows the confidence interval. Gene ontology (GO) enrichment analysis of DEPs and differentially expressed genes (DEGs) after (**D**) 30 days and (**E**) 60 days of storage of freeze-dried cells. The x-axis represents the GO term, and the y-axis represents the enrichment ratio. The blue and green bars in the histograms represent DEPs and DEGs, respectively. * FDR < 0.05; ** FDR < 0.01; *** FDR < 0.001. KEGG enrichment analysis of identified differential DEPs and DEGs at the two storage time points: (**F**) 30 days and (**G**) 60 days. Each circle represents a specific KEGG pathway, with the size and color of the circle indicating the number of significant DEGs/DEPs in that KEGG pathway and FDR, respectively.

Integrated analysis of proteomic and transcriptomic changes in the stored freeze-dried mutant strain

To identify the changes in the stored freeze-dried mutant strain from a combined proteomic and transcriptomic perspective, we conducted integrative GO and KEGG enrichment analyses on DEPs and DEGs specific to each storage time point (Fig. 3D-G). The GO enrichment analysis revealed 28 and 49 consistently enriched GO terms in the mutant compared to the wild-type on days 30 and 60 of storage, respectively (Fig. 3D, E). Notably, on both days, the top three significantly enriched GO functions in the mutant were the de novo IMP biosynthetic process, IMP metabolic process, and

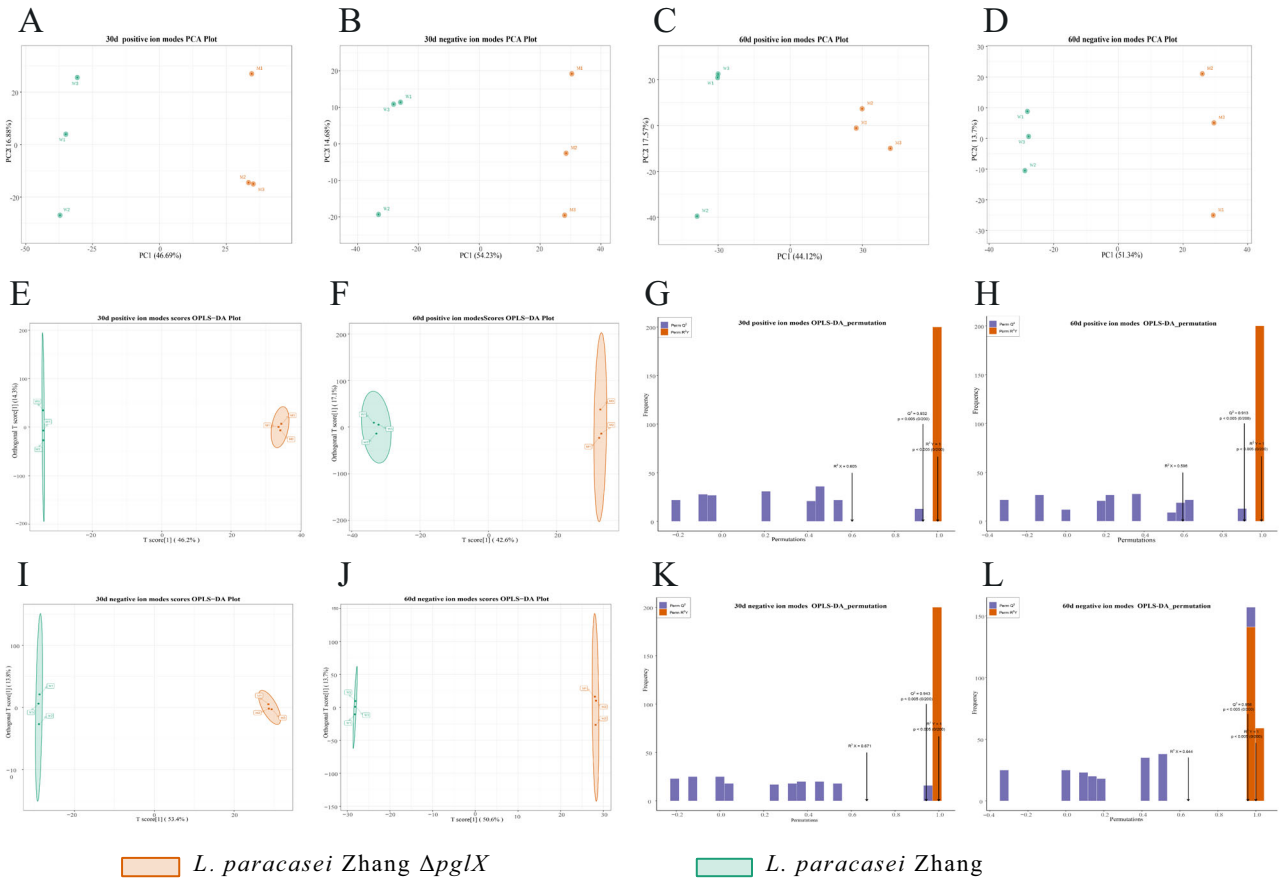

Fig. 4 | Metabolomics analysis results obtained at two storage time points (30 days and 60 days). Principal component analysis of metabolomics data generated in positive and negative ion modes at the two storage time points: (**A**, **C**) 30 days and (**B**, **D**) 60 days, respectively. Plots of OPLS-DA and permutation test (200 random permutations) of metabolomics data generated in positive ion mode at the two storage time points: (**E**, **G**) 30 days and (**F**, **H**) 60 days, respectively. Plots of OPLS-DA and permutation test (200 random permutations) of metabolomics data generated in negative ion mode at the two storage time points: (**I**, **K**) 30 days and (**J**, **L**) 60 days, respectively.

IMP biosynthetic process. In the KEGG enrichment analysis, several mutant-specific pathways were identified at both the proteomic and transcriptomic levels. On day 30, the enriched pathways included PTS (46 DEPs and 16 DEGs). On day 60, the enriched pathways included biofilm formation - *Escherichia coli* (four DEPs and three DEGs), pyruvate metabolism (12 DEPs and eight DEGs), and PTS (46 DEPs and 21 DEGs; Fig. 3F-G).

Untargeted metabolomics of freeze-dried cells stored post-storage

Untargeted metabolomics analysis was performed to detect post-storage metabolomic changes in freeze-dried mutant cells. Principal component analysis results indicated similar clustering patterns in the metabolomic datasets of both 30-day and 60-day stored samples, in both positive and negative ion modes (Fig. 4A-D). The distribution of symbols in the PCA plots revealed clear distinctions in metabolomic profiles between the stored freeze-dried wild-type and mutant cells, with wild-type cells on the left and mutant cells on the right, suggesting noticeable metabolomic differences between the two strains. The obtained metabolomics data were then subjected to OPLS-DA modeling and permutation tests (Fig. 4E-L). The OPLS-DA results revealed distinct bacterial strain-based clustering, suggesting significant metabolomic differences between the stored freeze-dried wild-type and mutant cells at both time points (Fig. 4E, F; I, J). The cumulative R^2X, R^2Y, and Q^2 values of the orthogonal partial least squares discriminant analysis (OPLS-DA) model between the freeze-dried wild-type and mutant cell metabolomes were: after 30 days of storage, 0.605, 1, and 0.932 (positive ion mode) and 0.671, 1, and 0.943 (negative ion mode); after 60 days of storage, 0.598, 1, and 0.913 (positive ion mode) and 0.644, 1, and 0.958 (negative ion mode). The R^2X and R^2Y values represent the model's explanatory power, while the Q^2 value indicates its predictive ability. Our data suggested that the OPLS-DA models generated from the current metabolomics datasets showed satisfactory fitness and predictability, and permutation tests (200 times) confirmed that their accuracy ($p < 0.05$; Fig. 4G, H; K, L).

Significantly differential metabolites between groups were defined by a variable importance in a projection score > 1 (from OPLS-DA models) and $p < 0.05$ (*t*-tests). The number of significantly differential metabolites between wild-type and mutant freeze-dried cells stored for 30 days, which included 358 increased and 566 decreased metabolites (positive ion mode); 381 increased and 362 decreased metabolites (negative ion mode). For 60-day stored cells, the number of significantly differential metabolites included 268 increased and 518 decreased metabolites (positive ion mode); 356 increased and 299 decreased metabolites (negative ion mode).

Further KEGG enrichment analysis on the identified significantly differential metabolites revealed some similarities and differences in enriched pathway profiles between the 30-day and 60-day storage metabolomic datasets. For example, the mutant strain showed enrichment in several pathways at both time points compared to the wild-type, including tryptophan metabolism (positive ion mode), two-component system, carbon metabolism, fructose and mannose metabolism, and butanoate metabolism (negative ion mode). In contrast, the stored mutant cells exhibited a significant reduction in amino acids and carbohydrates compared to the stored wild-type cells, suggesting a higher metabolic demand and increased consumption of these substrates during storage in the mutant strain. This is consistent with the observation of a previous report[25].

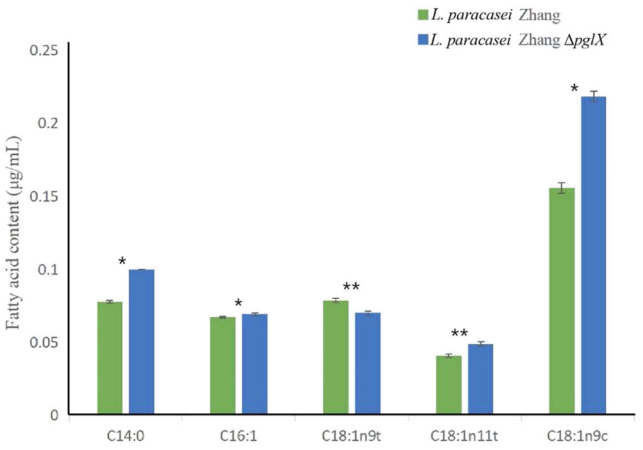

Fig. 5 | Membrane fatty acid contents in freeze-dried cells of *L. paracasei* Zhang (wild-type) and *L. paracasei* Zhang Δ*pglX* (mutant) after storage for 60 days. Error bars represent standard deviations. Significant differences between groups are indicated by: $^{*}p < 0.05$ and $^{**}p < 0.01$, respectively.

Targeted quantification of fatty acids and energy metabolism-related metabolites in freeze-dried cells

Targeted metabolomics analyses were conducted to quantify a specific set of metabolites in freeze-dried wild-type and mutant cells post-storage. This included 51 fatty acids (Table S1) and 68 energy-metabolism-related metabolites (Table S2). Our analysis revealed no significant alterations in the levels of targeted fatty acids after 30 days of storage ($p < 0.05$). However, a notable increase was observed in five fatty acids after 60 days (Fig. 5), specifically myristic acid (C14:0), palmitoleic acid (C16:1), elaidic acid (C18:1n9t), vaccenic acid (C18:1n11t), and oleic acid (C18:1n9c). With the exception of myristic acid (C14:0), which is a saturated fatty acid, all the significantly increased fatty acids were unsaturated.

A consistent pattern of metabolite changes was observed after both 30 and 60 days of storage (Table 1). Out of 65 targeted energy metabolism-related metabolites, 19 exhibited a similar trend of change at both time points, with 11 metabolites increasing and eight decreasing. The increased metabolites included xyluose-5-phosphate, acetyl-CoA, D-fructose-6-phosphate, D-glucose-1-phosphate, sedoheptulose-7-phosphate, D-glucose-6-phosphate, D-erythrose 4-phosphate, fructose-1,6-bisphosphate, trehalose-6-phosphate, glyceraldehyde-3-phosphate, and dihydroxyacetone-phosphate. The decreased metabolites included glutamine, malic acid, dUMP, dCMP, inosine, uracil, citric acid, and oxaloacetate. Two of the metabolites, namely glycerol-3-phosphate and itaconic acid, increased only after 30 days but not 60 days of storage.

Discussion

This study explored the role of adenine unmethylation in the stress response of the *L. paracasei* Zhang strain, particularly focusing on the Δ*pglX* mutant, to analyze its protective effects against freeze-drying. We conducted a comprehensive analysis of the post-storage changes in freeze-dried starter cultures at the transcriptomic, proteomic, and metabolomic levels. Our study demonstrated that adenine unmethylation significantly enhances the viability and survival rate of *L. paracasei* Zhang following freeze-drying, modulating gene expression and altering the cellular metabolome over varying storage durations.

Differentially expressed genes, proteins, and metabolites across various metabolic pathways were observed in the unmethylated strain after post-freeze-drying storage for different durations (Tables 2, 3). At both storage time points, the mutant strain showed notably enriched expression in PTS. On day 30, 12 of the 46 proteins and 16 genes in the PTS pathway were enriched, involving various PTS transport carbohydrate families, including the glucose (Glc), fructose (Fru), mannose (Man), and galactitol (Gat). Five genes showed increased expression: *bglF* (LCAZH_RS02965; both a kinase and a phosphatase responsible for the transport of β-glucoside in the Glc family[26]); *agaF* (LCAZH_RS13395; a PTS system mannose-specific transporter subunit IIA involved in phosphorylating carbohydrates in the Man family[27]); *gatC* (LCAZH_RS03235; a galactose PTS system EIIC component that participates in phosphorylating galactose in the Gat family[28]); *fruK* (LCAZH_RS13210; responsible for producing fructose-l,6-bisphosphate through ATP-dependent phosphorylation of fructose-l-phosphate[29], also participating in fructose and mannose metabolism); and *manY* (LCAZH_RS14305; a PTS system mannose-specific transporter subunit IIC, participating in mannose phosphorylation[30]). Apart from LCAZH_RS14305, the expression of the other four genes consistently increased at the protein level. Conversely, decreased expression was observed in seven genes: *cmtB* (LCAZH_RS14555; involved in the phosphorylation of mannitol in the Fru family[31]); *manY*, *manZ*, and *manXa* (LCAZH_RS02390, LCAZH_RS02395, LCAZH_RS02405, respectively; components of transporters responsible for transporting mannose[30]); *gatA* and *gatB* (LCAZH_RS13340, LCAZH_RS13335; components of transporters responsible for transporting galactitol[32]); and *agaF* (LCAZH_RS02230; an N-acetylgalactosamine PTS system EIIA component responsible for phosphorylating N-acetylgalactosamine[27]).

On day 60, 16 of the 46 proteins and 21 genes in the PTS pathway were enriched, with five proteins maintaining increased expression from day 30 to day 60. Ten genes showed decreased expression on day 60, six of which continued the downward trend on day 30 (i.e., LCAZH_RS14555, LCAZH_RS02390, LCAZH_RS02395, LCAZH_RS13340, LCAZH_RS13335, and LCAZH_RS02230). Four genes displayed inconsistent trends on days 30 and 60, which were: *celB* and *celC* (LCAZH_RS14220, LCAZH_RS14235, respectively; components of the cellobiose PTS system involved in cellobiose/diacetylchitobiose phosphorylation[33]); *manX* and *manY* (LCAZH_RS02235, LCAZH_RS02245, respectively; mannose PTS system components responsible for mannose transport[30]), showing decreased transcription but increased protein expression, which suggests complex regulation of these genes. The consistent upregulation of five PTS families in gene expression, despite occasional transcriptional contradictions (Fig. 6), indicates a potential physiological response to enhance sugar import and improve carbohydrate utilization and energy metabolism in freeze-dried cells, especially in the mutant strain after extended storage. The role of PTS role in facilitating the uptake and phosphorylation of sugars is crucial for cellular growth and metabolism, and its upregulation may reflect an adaptive mechanism to stress conditions.

The metabolites released by probiotics are known to play a pivotal role in bacterial life activities and stress responses[34,35]. This study monitored the changes in metabolites during the storage of *L. paracasei*, which are crucial for cells to adapt to stressful environment. Non-targeted metabolomics revealed significant decreases in several carbohydrate metabolites, such as D-mannitol, rhamnose, and D-maltose, suggesting a shift in carbohydrate metabolism. Conversely, sugar phosphates like trehalose-6-phosphate, D-sorbitol-6-phosphate, and D-mannitol-1-phosphate increased significantly, indicating an active response to stress. Trehalose-6-phosphate, an intermediate in trehalose catabolism, is produced intracellularly and plays a role in energy metabolism and stress protection[36]. The increase in trehalose-6-phosphate in both non-targeted and targeted metabolomics analyses supports its importance in cellular adaptation. Both mannitol and sorbitol are PTS sugar substrates[37]. Efiuvwevwere et al. demonstrated that mannitol provides osmotic protection and exhibits antioxidant effects on *Lactococcus lactis*, leading to decreased water activity and improved survival of dried starter cultures[38]. Many lactic acid bacteria can utilize mannitol and sorbitol via PTS. D-mannitol and D-sorbitol are simultaneously absorbed and phosphorylated by PTS proteins to form D-mannitol-1-phosphate and D-sorbitol-6-phosphate[39,40]. The results indicate that the increased survival rate of the mutant strain is likely linked to its enhanced carbohydrate metabolism[21,23,25].

In addition to carbohydrates, differences in intermediate metabolites involved in core metabolic pathways were observed between wild-type and

Table 1 | Differential energy metabolites identified between freeze-dried *Lacticaseibacillus paracasei* Zhang wild-type and mutant cells after 30 and 60 days of storage

Metabolite	Retention time (min)	*p*-value		Fold change		Trend
		30 d	60 d	30 d	60 d	
Glutamine	5.73	0.000006744	0.0005620	0.48	0.49	down
Malic acid	4.71	0.000048064	0.0001308	0.26	0.26	down
Xyluose-5-phosphate	5.91	0.000861652	0.0287859	2.21	2.59	up
Acetyl-CoA	5.81	0.000906987	0.0023236	2.54	3.01	up
dUMP	5.37	0.000000057	0.0008983	0.18	0.18	down
dCMP	6.23	0.000442553	0.0000940	0.43	0.42	down
Inosine	1.98	0.000096385	0.0001332	0.16	0.16	down
Uracil	1.08	0.000000207	0.0000107	0.28	0.28	down
Citric acid	6.91	0.000873181	0.0001554	0.00	0	down
Oxaloacetate	0.76	0.003319451	0.0090368	0.23	0.18	down
D-Fructose-6-phosphate	6.61	0.000037653	0.0084723	2.40	2.40	up
D-Glucose-1-phosphate	6.62	0.001440232	0.0008947	2.34	2.23	up
Sedoheptulose-7-phosphate	5.71	0.000062777	0.0002287	Inf	Inf	up
D-Glucose-6-phosphate	6.55	0.000091896	0.0027521	5.09	5.57	up
D-Erythrose-4-phosphate	6.26	0.000668358	0.0008812	9.23	10.44	up
Fructose-1,6-bisphosphate	7.87	0.000061262	0.0001430	4.35	4.73	up
Trehalose-6-phosphate	7.67	0.000535995	0.0000061	2.43	2.18	up
Glyceraldehyde-3-phosphate	5.74	0.000045585	0.0000105	Inf	Inf	up
Dihydroxyacetone-phosphate	5.75	0.000130780	0.0001212	Inf	Inf	up

Remark: Data presented in this table were generated by targeted metabolomics of energy metabolism-related metabolites.

mutant cells post-storage. Pyruvate, a key intermediate in energy metabolism and biosynthesis, is central to lactic acid and acetyl coenzyme A production[41]. Under acidic stress, bacteria can modulate amino acid metabolism to convert amino acids into pyruvate, thereby enhancing lactic acid production and providing additional energy to counteract acid stress[42]. *OadA* (LCAZH_RS09370) encodes an oxaloacetate decarboxylase that efficiently catalyzes the decarboxylation of oxaloacetate into pyruvate during pyruvate metabolism[43]. In the mutant cells, the expression of *OadA* was enhanced, correlating with reduced oxaloacetate levels observed in the metabolomics analysis. Moreover, four enzymatic components of the pyruvate dehydrogenase complex (*pdhA*, LCAZH_RS06625; *pdhB*, LCAZH_RS06630; *pdh*C, LCAZH_RS06635; *pdh*D, LCAZH_RS06640), encoding the pyruvate dehydrogenase major (E1α) and minor (E1β) subunits, dihydrolipoyl acetyltransferase (E2), and dihydrolipoyl dehydrogenase (E3)[44], showed consistently increased expression. Pyruvate is converted irreversibly into acetyl coenzyme A through the action of the pyruvate dehydrogenase complex. This is consistent with targeted metabolomics findings, which revealed higher levels of acetyl coenzyme A in stored mutant cells. Acetyl coenzyme A, a crucial intermediate metabolite in energy metabolism, is subsequently converted into malonyl coenzyme A by the acetyl coenzyme A carboxylase (ACC) complex during the initial stages of fatty acid biosynthesis.

Interestingly, the components of the ACC complex, including *accA* (LCAZH_RS10410), *accB* (LCAZH_RS10435), *accC* (LCAZH_RS10425), and *accD* (LCAZH_RS10415), were significantly upregulated at the transcriptomic level but not at the proteomic level in the mutant at both storage time points. The ACC complex plays a pivotal role in fatty acid synthesis. An *Escherichia coli* strain engineered to overexpress ACC showed a six-fold increase in fatty acid levels[45]. Co-overexpressing multiple genes, including *accA* and *fabD*, can enhance fatty acid production in both *Pseudomonas aeruginosa* and *Escherichia coli*[46], aligning with the current observation of elevated fatty acid production in the stored mutant cells. The mutant strain also exhibited a notable increase in the level of oleic acid (C18:1n9c), which may be attributed to the enhanced expression of the ACC complex. The ACC complex is key and rate-limiting enzyme in fatty acid synthesis[47]; therefore, its elevated expression can lead to accelerated fatty acid synthesis. Previous studies have reported that the survival of some lactic acid bacteria, such as *Lactiplantibacillus plantarum* and *Lactobacillus acidophilus*, during storage and freeze-drying is influenced by the fatty acid composition of the bacterial membrane[48–51]. The enhanced expression of genes related to fatty acid synthesis may represent a survival strategy for *L. paracasei* under the harsh conditions. Particularly, since variations in cellular fatty acid content can substantially alter the physical properties of bacterial cell membranes[52]. Thus, it is logical to speculate that the improved survival of the mutant post-freeze-drying could be due to increased cell membrane strength, driven by the action of the ACC complex in promoting fatty acid synthesis.

Similarly, the increased expression of *fabZ* (LCAZH_RS10430, LCAZH_RS10475), *fabK* (LCAZH_RS10455), and *fabH* (LCAZH_RS10465) in response to environmental stress aligns with a previous report that the *L. paracasei* A13 strain responds to high-pressure stress by overexpressing some of these genes[53]. The *fab* gene cluster is responsible for the biosynthesis of unsaturated fatty acids as well as the early stages of fatty acid synthesis. In particular, the *fabZ* gene encodes β-hydroxyacyl-acyl carrier protein dehydratase, which plays a role in producing unsaturated fatty acids[54]. The *fabH* gene encodes β-ketoacyl-acyl carrier protein synthase III, which catalyzes the initial condensation reactions necessary for bacterial type II fatty acid biosynthesis[55]. In our analysis, the expression of the *fabH* gene in the mutant strain was 6.81 times higher than in the wild-type cells. This increase in the fatty acid synthesis pathway in the mutant strain supports the hypothesis that lactic acid bacteria adapt their fatty acid synthesis pathways to survive in extreme conditions[56,57]. Furthermore, the differences in regulation of the fatty acid synthesis pathway between the mutant and wild-type strains suggest that DNA methylation status plays a role in influencing the expression of these metabolic pathways. This, in turn, affects the ability of the cells to withstand stress.

Metabolomics analysis revealed significant increases in several free fatty acids, including 2-hydroxyhexadecanoic acid, dodecanedioic acid, 16-hydroxyhexadecanoic acid, epoxyoleic acid, floionolic acid, ricinoleic acid, 12-hydroxystearic acid, bovinic acid, oleic acid, and 9-hexadecenoic acid, in

Table 2 | Differential expressed genes (DEGs) and proteins (DEPs) identified between freeze-dried *Lacticaseibacillus paracasei* Zhang wild-type and mutant cells after 30 and 60 days of storage

Locus_tag	Gene	Description	Fold change			
			DEP		DEG	
			30 d	60 d	30 d	60 d
LCAZH_RS02965	*bglF*	PTS glucose transporter subunit IIA	1.62	1.64	8.97	8.08
LCAZH_RS13395	*agaF*	PTS fructose transporter subunit IIA	2.68	2.50	3.54	4.10
LCAZH_RS03235	*gatC*	PTS glucitol transporter subunit IIA	1.86	1.64	3.06	3.01
LCAZH_RS13210	*fruK*	1-phosphofructokinase	1.53	1.53	2.88	2.29
LCAZH_RS14305	*manY*	PTS mannose/fructose/sorbose transporter subunit IIC	0.61	0.54	6.64	4.74
LCAZH_RS14555	*cmtB*	PTS sugar transporter subunit IIA	1.82	1.84	0.11	0.14
LCAZH_RS02390	*manY*	PTS sugar transporter subunit IIC	2.43	2.25	0.20	0.20
LCAZH_RS02395	*manZ*	PTS system mannose/fructose/sorbose family transporter subunit IID	2.98	2.85	0.20	0.19
LCAZH_RS02405	*manXa*	PTS N-acetylglucosamine transporter subunit IIBC	2.31	2.19	0.50	0.46
LCAZH_RS13340	*gatA*	PTS sugar transporter subunit IIA	3.36	3.21	0.17	0.14
LCAZH_RS13335	*gatB*	PTS galactitol transporter subunit IIB	5.32	4.81	0.15	0.11
LCAZH_RS02230	*agaF*	fructose/mannose phosphotransferase system IIA component	6.32	5.48	0.11	0.10
LCAZH_RS13400	*agaE*	PTS system mannose/fructose/sorbose family transporter subunit IID	2.85	2.77	2.53	3.16
LCAZH_RS14220	*celB*	Oligo-beta-mannoside permease IIC component	1.90	2.02	2.08	0.63
LCAZH_RS14235	*celC*	PTS lactose/cellobiose transporter subunit IIA	2.25	2.12	2.16	0.24
LCAZH_RS09370	*oadA*	oxaloacetate decarboxylase subunit alpha	2.27	2.20	5.05	4.80
LCAZH_RS06625	*pdhA*	pyruvate dehydrogenase (acetyl-transferring) E1 component subunit alpha	3.58	3.48	1.32	1.28
LCAZH_RS06630	*pdhB*	alpha-ketoacid dehydrogenase subunit beta	3.42	3.35	2.30	1.89
LCAZH_RS06635	*pdhC*	dihydrolipoyllysine-residue acetyltransferase	3.91	3.76	2.10	2.19
LCAZH_RS06640	*pdhD*	dihydrolipoyl dehydrogenase	3.38	3.32	3.71	3.04
LCAZH_RS10410	*accA*	acetyl-CoA carboxylase carboxyl transferase subunit alpha	1.53	1.40	6.23	7.05
LCAZH_RS10435	*accB*	acetyl-CoA carboxylase biotin carboxyl carrier protein	0.98	0.98	10.69	15.83
LCAZH_RS10425	*accC*	acetyl-CoA carboxylase biotin carboxylase subunit	1.11	1.12	5.81	5.78
LCAZH_RS10415	*accD*	acetyl-CoA carboxylase carboxyltransferase subunit beta	1.39	1.37	5.24	5.65
LCAZH_RS10430	*fabZ*	3-hydroxyacyl-ACP dehydratase	1.23	1.16	8.91	8.94
LCAZH_RS10475	*fabZ*	beta-hydroxyacyl-ACP dehydratase	1.10	1.08	16.40	15.28
LCAZH_RS10455	*fabK*	nitronate monooxygenase	1.14	1.15	10.40	8.52
LCAZH_RS10465	*fabH*	ketoacyl-ACP synthase III	1.01	1.05	6.81	6.43
LCAZH_RS13840	*asdA*	aspartate 4-decarboxylase	1.12	1.11	3.31	3.38
LCAZH_RS08840	*purQ*	phosphoribosylformylglycinamidine synthase subunit PurQ	0.21	0.27	0.24	0.31
LCAZH_RS08830	*purF*	amidophosphoribosyltransferase	1.31	1.35	0.16	0.21

the unmethylated mutant strain. These findings suggest that the mutant relies on fatty acid metabolism to adapt to environmental stress. The presence of unsaturated fatty acids like ribcinoleic acid, bovinic acid, oleic acid, and 9-hexadecenoic acid among the differentially abundant free fatty acids is particularly noteworthy. The unsaturation index of membrane fatty acids influences membrane viscosity and thickness, thereby controlling membrane permeability[58,59]. It has been shown that unsaturated fatty acid synthesis increases in *Lactobacillus acidophilus* RD758 when adapting to low-temperature stress[60]. Oleic acid, in particular, plays a significant role in the growth and survival of lactobacilli[61], as its biosynthesis increases the proportion of unsaturated to saturated fatty acids[62]. Our results suggest that the formation of vaccenic acid from palmitoleic acid may occur through unsaturated fatty acid synthesis[63], independent of oxygen, thus altering the unsaturation level of fatty acids[64,65]. This process may be crucial for the mutant's adaptation to stress conditions.

In addition to carbohydrate and fatty acid metabolism, changes in amino acid content may also contribute to protection against storage stress. Several amino acids and their derivatives were found to decrease in the stored mutant cells after 30 and 60 days of storage compared to the wild-type. Specific amino acids, such as arginine, tryptophan, and leucine, are essential for regulating central metabolic pathways needed for maintenance, growth, and reproduction[66]. The reduction in L-aspartic acid was accompanied by an increase in aspartate 4-decarboxylase (*asdA*, LCAZH_RS13840), which converts L-aspartate to L-alanine. Meanwhile, the level of L-glutamic acid decreased significantly, with modulated expression of alanine, aspartate, and glutamate metabolism-related genes and proteins. Specifically, the transcriptomic and proteomic expression of *purQ* (LCAZH_RS08840) decreased; it encodes a glutaminase that converts glutamine to glutamate to produce ammonia[67]. Additionally, *PurF* (LCAZH_RS08830) catalyzes the formation of phosphoribosylamine from glutamine[68]. This gene was significantly downregulated at the transcriptional level in the mutant at both storage time points, although no changes were observed at the proteomic level. Notably, *purF* also catalyzes the initial reaction of purine metabolism.

Materials and methods

Frozen bacterial stock and reactivation

The Key Laboratory of Dairy Biotechnology and Engineering, Ministry of Education, Inner Mongolia Agricultural University, provided the frozen

Table 3 | Differential metabolites identified between freeze-dried *Lacticaseibacillus paracasei* Zhang wild-type and mutant cells after 30 and 60 days of storage

Metabolite	Actual Mass (m/z)	Retention time (min)	VIP score		*p*-value		Fold change	
			30 d	60 d	30 d	60 d	30 d	60 d
Trehalose-6-phosphate	422.08	1.23	1.35	1.4	0.0008055	0.001187	2.36	2.36
D-Sorbitol-6-phosphate	261.04	0.72	1.36	1.39	0.0010906	0.0000037	40.85	50.48
D-Mannitol-1-phosphate	261.04	1.03	1.33	1.17	0.0007905	0.0069542	148.15	11.44
Mannitol	241.11	5.01	1.23	1.26	0.0246834	0.0359189	0.73	0.78
Rhamnose	201.03	0.61	1.37	1.4	0.0000064	0.001824	0.69	0.7
D-Maltose	409.07	0.64	1.45	1.47	0.0188156	0.0360397	0.39	0.3
2-Hydroxyhexadecanoic acid	543.46	10.23	1.18	1.32	0.0266746	0.0111031	1.54	1.85
Dodecanedioic acid	229.16	2.21	1.34	1.36	0.0005394	0.0031792	1.25	1.25
16-Hydroxyhexadecanoic acid	271.23	8.87	1.37	1.29	0.0004318	0.010989	2.02	1.6
Epoxyoleic acid	297.24	9.35	1.33	1.28	0.0008873	0.0474424	1.34	1.35
Floionolic acid	331.25	6.58	1.34	1.38	0.0005649	0.0005442	7.82	7.46
Ricinoleic acid	357.26	9.18	1.16	1.23	0.0336	0.0264366	1.12	1.12
12-Hydroxystearic acid	299.26	9.92	1.28	1.32	0.0205865	0.0181527	1.27	1.31
Bovinic acid	245.22	9.34	1.42	1.45	0.0203537	0.0057509	1.3	1.38
Oleic acid	247.24	9.9	1.46	1.46	0.0003216	0.014457	1.32	1.26
9-Hexadecenoic acid	255.23	8.86	1.47	1.49	0.0004307	0.0045631	2.07	1.74
Arginine	175.12	0.83	1.4	1.44	0.0033395	0.016441	0.71	0.73
L-Tryptophan	205.1	2.49	1.42	1.52	0.0126646	0.0004172	1.87	1.56
DL-Leucine	132.1	1.77	1.28	1.51	0.0223176	0.0044968	1.19	1.2
L-Aspartic acid	132.03	0.73	1.36	1.39	0.0001659	0.0068734	0.49	0.49
L-Glutamic acid	146.05	0.74	1.36	1.38	0.0005801	0.0027066	0.74	0.75

Remark: Data presented in this table were generated by untargeted metabolomics analysis.

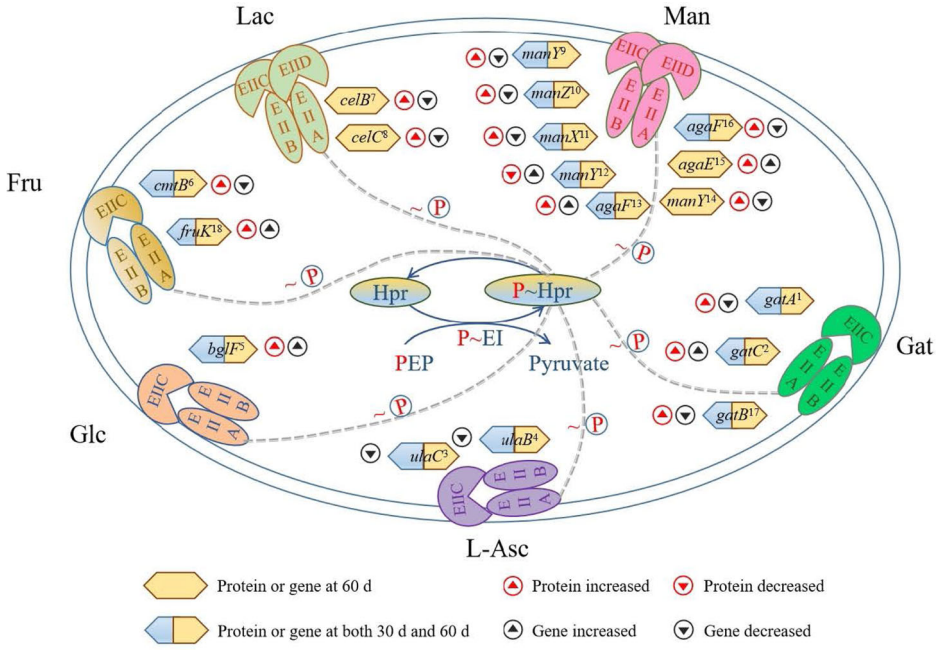

Fig. 6 | Changes in protein and gene expression of phosphotransferase system (PTS) components at the two storage time points (30 and 60 days). Glc = glucose; Fru = fructose; Lac = lactose; Man = mannose; Gat = galactitol; L-Asc = L-ascorbate; P = phosphate; EI = enzyme I; Hpr = histidine phosphate carrier protein; EIIABCD = enzyme II complex. The superscript number after the protein or gene represents the locus tag (1: LCAZH_RS13340, 2: LCAZH_RS03235, 3: LCAZH_RS13630, 4: LCAZH_RS13635, 5: LCAZH_RS02965, 6: LCAZH_RS14555, 7: LCAZH_RS14220, 8: LCAZH_RS14235, 9: LCAZH_RS02390, 10: LCAZH_RS02395, 11: LCAZH_RS02405, 12: LCAZH_RS14305, 13: LCAZH_RS13395, 14: LCAZH_RS02245, 15: LCAZH_RS13400, 16: LCAZH_RS02230, 17: LCAZH_RS13335, 18: LCAZH_RS13210).

glycerol stocks of *L. paracasei* Zhang and the Δ*pglX* mutant strains. These strains were revived and purified using the streak-plate method to ensure isolation of individual colonies. Representative colonies were picked and subcultured in MRS broth at 37 °C for 24 h[69].

Preparation and storage of freeze-dried starter cultures

The reactivated cultures were grown in a modified MRS medium maintained at a constant pH of 5.9 within a fermenter until the optical density at 600 nm (OD_{600}) reached a plateau, indicating the end of exponential

growth. Cells were harvested by centrifugation at 4 °C for 15 min. A freeze-drying protective agent was then added to cell pellet of each strain, thoroughly mixed, and subjected to a pre-chilling step at -80 °C for 72 h. The cell suspensions were subsequently freeze-dried using a vacuum freeze-dryer (DRC-1000, EYELA, Tokyo, Japan) for 20 h, with a cold trap temperature at -60 °C and a vacuum pressure maintained at 5 Pa. The viability of the freeze-dried starter bacterial cells was determined, and the survival rate through the freeze-drying process was calculated. Then, the starter cultures were stored at 30 °C, and the bacterial viability was measured after 30 and 60 days of storage.

Assessment of viability and survival of freeze-dried starter cultures

The viability of the freeze-dried starter cultures was assessed using the plate count method. Samples of freeze-dried bacterial starters (1 g per sample), collected at 0, 30, and 60 days of storage, were serially diluted in 99 mL of normal saline solution. A 10-fold dilution series was prepared, with each subsequent dilution prepared by mixing 0.5 mL of the bacterial solution with 4.5 mL of normal saline, up to a dilution of 10^{-9}. For the plate count, 1 mL aliquots from the dilution series were plated in triplicate. After incubating the inoculated plates at 37 °C for 24 h, those with colonies within the countable range of 30 to 300 were enumerated. The survival rate of the freeze-dried cultures was calculated using the following formula:

$$\text{Survival rate after freeze} - \text{drying}(\%) = (N_1/N_0) \times 100\%,$$

where N_0 was the initial count of viable bacteria before freeze-drying, and N_1 was the count of viable bacteria after freeze-drying.

Preparation of freeze-dried cells for omics analyses

Following storage for designated durations of 30 and 60 days, freeze-dried starter cultures of each cell line (5 g per sample) were preserved at -80 °C for subsequent transcriptomics, proteomics, and metabolomics analyses. Three biological replicates were prepared in parallel.

Extraction of RNA, library preparation, and Illumina sequencing

We extracted the total RNA from the cell pellets collected after 30 and 60 days of storage using Invitrogen TRIzol® Reagent (Carlsbad, CA, USA) following the recommended procedures of the manufacturer. Genomic DNA was eliminated using DNase I (TaKara Bio USA, Inc., San Jose, CA, USA), and the quantity and quality of the extracted RNA were assessed using an Agilent 2100 bioanalyzer (Agilent Technologies Co., Ltd., Santa Clara, CA, USA) and a NanoDropTM 2000 spectrophotometer (Thermo Fisher Scientific, Waltham, MA, USA). The TruSeqTM RNA Sample Preparation Kit (Illumina Inc., San Diego, CA, USA) was used to create RNA-sequencing libraries, and the Ribo-zero Magnetic Kit (Epicentre Biotechnologies, Madison, WI, USA) was employed to deplete rRNA, followed by random fragmentation of mRNA into approximately 200 bp fragments. Double-stranded cDNA was synthesized using the Invitrogen SuperScript Double-stranded cDNA Synthesis Kit (Invitrogen Corporation, Carlsbad, CA, USA) with Illumina random primers (Illumina, Inc., San Diego, CA, USA). End repair, phosphorylation, and adapter ligation were performed, followed by the removal of second-strand cDNA using uracil N-glycosylase (Thermo Fisher Scientific, Waltham, MA, USA). The library was enriched, amplified through 15 cycles of PCR with the Phusion DNA Polymerase (New England Biolabs, Ipswich, MA, USA), and quantified using a TBS380 mini-fluorometer (Invitrogen, Corporation, Carlsbad, CA, USA). RNA-sequencing was conducted using an Illumina Hiseq x Ten system, generating 2 × 150 bp paired-end reads (Shanghai Majorbio Bio-Pharm Technology Co., Ltd., Shanghai, China).

Bioinformatics analysis of transcriptomics data

High-quality sequencing reads were aligned to the reference genome (NCBI assembly ID GCF_000019245.4) using Bowtie2 (http://bowtie-bio.sourceforge.net/bowtie2/index.shtml). Gene transcription levels were estimated with the RSEM tool (http://deweylab.github.io/RSEM/), and differentially expressed genes (DEGs) were identified using the DESeq2 tool (http://bioconductor.org/packages/release/bioc/html/DESeq2.html), with a significance threshold of false discovery rate (FDR) < 0.05 and fold change (FC) ≥ 2 or ≤ 0.5. Functional enrichment analyses were performed using GO (http://geneontology.org/) and KEGG (https://www.genome.jp/kegg/) databases, with significant enrichment defined by an FDR < 0.05.

Protein extraction and trypsinization

Samples were pulverized in liquid nitrogen and ultrasonicated in a pyrolysis buffer containing 1% sodium deoxycholate and 8 M urea on ice. The resulting cell extracts were centrifuged to collect the supernatants. The Pierce™ BCA Protein Assay Kit (Thermo Fisher Scientific, Waltham, MA, USA) was employed to quantify the protein content. To reduce disulfide bonds, tris(2-carboxyethyl) phosphine was added to the samples at a final concentration of 10 mM, and the mixture was incubated at 37 °C for 1 h. Then iodine acetamide was added at a final concentration of 40 mM, kept in a light-free environment at room temperature for 40 min. Subsequently, the samples were precipitated by the adding six volumes of chilled acetone, left to stand at -20 °C for 4 h before centrifugation. The resulting pellets were resuspended in a 50 mmol/L triethylammonium bicarbonate buffer. The extracted protein was subjected to overnight trypsinization at 37 °C with a trypsin: protein mass ratio of 1:50.

Tandem mass tag (TMT) labeling and liquid chromatography-tandem mass spectrometry (LC-MS/MS) analysis

The TMT labeling procedure was modified from a previous paper to improve efficiency and accuracy[70]. The process involved optimizing sample preparation, chromatographic conditions, and mass spectrometry settings. Refinements also included the use of an ultra-performance liquid chromatography system and a modified gradient elution program for better peptide separation.

The trypsinized peptides were labeled with TMT reagent (Thermo Fisher Scientific, Waltham, MA, USA) and incubated at room temperature for 2 h. An equal volume of hydroxylamine was added and left to incubate for 15 min, and the mixture was dried using a vacuum concentrator. The dried peptides were resuspended in an ultra-performance liquid chromatography loading buffer for separation using a 75 μm × 25 cm C18-reversed phase column (Thermo Fisher Scientific, Waltham, MA, USA). The chromatographic conditions were optimized with phase A consisting of 2% acetonitrile adjusted to pH 10 with ammonia, and phase B consisting of 80% acetonitrile adjusted to pH 10 with ammonia, at a flow rate of 200 μL/min. The peptides were consolidated into 10 fractions, concentrated by vacuum centrifugation, before analysis on an easy-nLC 1200 coupled with Q Exactive mass spectrometer (Thermo Fisher Scientific, Waltham, MA, USA). The peptides were reconstituted in a mass spectrometry (MS) buffer and subjected to a 2-h partition on a 75 μm × 25 cm C18 column (Thermo Fisher, Waltham, MA, USA) with a flow rate of 300 nL/min. The mobile phase consisted of phase A (2% acetonitrile and 0.1% formic acid) and phase B (80% acetonitrile and 0.1% formic acid). The gradient elution program was as follows: 0-67 min, 6-23% B; 67-81 min, 23-29% B; 81-90 min, 29-38% B; 90-92 min, 38-48% B; 92-93 min, 48-100% B; and 93-120 min, 100% B. Mass spectra were acquired in the range of 350-1500 (m/z) with a primary MS resolution of 120,000 and a secondary MS resolution of 45,000.

Bioinformatics analysis of proteomics data

Proteomic Discoverer™ software 2.4 was implemented to process and analyze the raw LC-MS/MS spectra, with a significant cut-off level of Benjamini-Hochberg method-corrected FDR of ≤ 0.01. Protein identification required at least one unique peptide segment. The FC and *p*-value comparisons between groups were performed using the *t*-test function in R. Differential expression analysis of proteins was conducted between two distinct samples.

The criteria for selecting significantly differentially expressed proteins (DEPs) were a *p*-value < 0.05 and FC > 1.5 for upregulated

DEPs; and a p-value < 0.05 with an FC < 0.67 for downregulated DEPs. The dataset and associated metabolic pathways were annotated and discerned using the GO (http://www.blast2go.com/b2ghome; http://geneontology.org/) for functional clustering analysis and the KEGG database (http://www.genome.jp/kegg/).

Liquid chromatography PRM protein analysis

Parallel reaction monitoring, known for its high specificity, sensitivity, and quantitative accuracy, was employed to validate DEPs in proteomic studies[71]. Following TMT proteomics, 14 target proteins were selected for PRM analysis. Sample separation was achieved a 75 μm × 25 cm C18 column (Thermo Fisher, Waltham, MA, USA) with the EASY-nLC 1200 liquid phase system. The MS resolution was set at 60,000, with an automatic gain control target of 3e6, normalized collision energy of 28, chromatographic peak width of 30 s, and an isolation window of 1.4 m/z.

Untargeted metabolomics

Samples were prepared for untargeted metabolomic analysis by thawing on ice and mixing 20 mg of each sample with 400 μL of 70% methanol containing an internal standard (Merck, Darmstadt, Hessen Land, Germany). The mixture was vortexed for three min, sonicated on ice for 10 min, vortexed again for 1 min, and then incubated at -20 °C for 30 min, before centrifugation at 12,000 rpm for 10 min at 4 °C. The supernatants were transferred to clean centrifuge tubes. Aliquots of 200 μL of supernatants were analyzed by LC-MS using a Waters ACQUITY UPLC HSS T3 C18 column (1.8 μm, 2.1 mm × 100 mm; Waters Corporation Milford, MA, USA). The LC-MS operating parameters included: a column temperature of 40 °C, a flow rate of 0.4 mL/min, and a solvent mixture of water and acetonitrile with 0.1% formic acid. The elution process started with 5% mobile phase B, consisting of 0.1% formic acid in acetonitrile, at 0 min, followed by a linear gradient to 90% mobile phase B over 11 min, held for 1 min, then a rapid return to 5% mobile phase B within 0.1 min, held for 1.9 min.

To facilitate analysis, ProteoWizard software was used to transform the initial data into mzML format. Unsupervised principal component analysis was performed using the prcomp function in R. Orthogonal partial least squares-discrimination analysis (OPLS-DA) was achieved using MetaboAnalystR, with data mean-centered to prevent overfitting and permutation tests with 200 permutations. Metabolite identification was facilitated by the KEGG Compound database (http://www.kegg.jp/kegg/compound/), with further comparison against the KEGG Pathway database (http://www.kegg.jp/kegg/pathway.html).

Targeted metabolomics of medium- and long-chain fatty acids

For the targeted analysis of medium- and long-chain fatty acids, 50 mg samples were precisely weighed and combined with a steel ball in a mixture of chloroform and methanol (1:1 v/v; 1 mL). The mixture was sonicated at 50 KHz for 3 min at 5 °C and then centrifuged at 13,000 × g for 10 min at 4 °C. An aliquot of 500 μL of the supernatant was treated with 0.5 mL of sodium hydroxide methanol solution (0.5 mol/L), vortex for 30 s, and incubated at 60 °C for 30 min. After cooling, 0.5 mL of n-hexane was added, vortexed for 30 s, and centrifuged at 13,000 × g at 4 °C for 10 min. The upper n-hexane layer (approximately 100 μL) was transferred to sample vials for analysis. The prepared samples were analyzed using an Agilent 8890B gas chromatography system equipped with an Agilent 5977B/7000D mass selective detector, operating at an ionization voltage of 70 eV (Agilent Technologies Co., Ltd., Santa Claria, CA, USA). An Agilent CP-Sil88 capillary column (100 m × 0.25 mm × 0.20 μm) was utilized for the separation of fatty acid methyl esters. The GC temperature program started at 80 °C, ramped to 180 °C at an 8 °C per min rate, further increased to 220 °C at 4 °C per min, then to 230 °C at 2 °C per min, maintained for 13.5 min, and finally held at 235 °C for 2 min. For sample injection, 1 μL was applied in split mode (50:1). The temperatures for the inlet, ion source, and quadrupole were set and held at 260 °C, 230 °C, and 150 °C, respectively.

Compounds were analyzed in scanning mode, and identification and quantification were performed using Masshunter software (v10.0.707.0; Agilent Technologies Co., Ltd., Santa Claria, CA, USA). Linear regression standard curves were constructed using the mass spectrum peak areas and analyte concentrations to estimate the concentrations of analytes of interest.

Targeted metabolomics of energy metabolism-related metabolites

For the analysis of energy metabolism-related metabolites, 50 mg samples were weighed and vortex mixed with 70% methanol (500 μL), followed by centrifugation at 12,000 rpm for 10 min at 4 °C). Then, supernatants (300 μL) were carefully collected, kept at -20 °C for 30 min, and recentrifuged for 10 min. Aliquots of 200 μL of the extracts were analyzed using a Waters ACQUITY H-Class LC-ESI-MS/MS system (Waters Corporation, Milford, MA, USA). Both linear ion trap and triple quadrupole scans were obtained by a QTRAP® 6500 + LC-MS/MS system. Significantly different metabolites between samples were identified based on variable importance in projection scores from OPLS-DA and absolute $\log_2$FC calculated using MetaboAnalystR. Data were mean-centered to prevent overfitting before performing OPLS-DA and permutation tests (200 permutations).

Data availability

Data are accessible through the NCBI Sequence Read Archive database (BioProject ID PRJNA994019 for raw transcriptomics data) and the ProteomeXchange Consortium database (iProX partner repository identifiers PXD043736 and PXD043735 for MS proteomics and PRM analysis data).

Received: 29 April 2024; Accepted: 10 March 2025;
Published online: 19 May 2025

References

1. Leroy, F. & De Vuyst, L. Lactic acid bacteria as functional starter cultures for the food fermentation industry. *Trends Food Sci. Technol.* **15**, 67–78, https://doi.org/10.1016/j.tifs.2003.09.004 (2004).
2. Bensch, G. et al. Flow cytometric viability assessment of lactic acid bacteria starter cultures produced by fluidized bed drying. *Appl. Microbiol. Biotechnol.* **98**, 4897–4909, https://doi.org/10.1007/s00253-014-5592-z (2014).
3. Broeckx, G., Vandenheuvel, D., Claes, I. J., Lebeer, S. & Kiekens, F. Drying techniques of probiotic bacteria as an important step towards the development of novel pharmabiotics. *Int J Pharm.* **505**, 303–318, https://doi.org/10.1016/j.ijpharm.2016.04.002 (2016).
4. Begum, R. et al. Isolation and characterization of lactic acid bacteria from indigenous dairy product and preparation of starter culture by freeze-drying. *BRC* **3**, 302–308, https://doi.org/10.1016/j.smallrumres.2021 (2017).
5. Wang, Z. et al. A comprehensive review on stability of therapeutic proteins treated by freeze-drying: induced stresses and stabilization mechanisms involved in processing. *Dry. Technol.* **40**, 3373–3388, https://doi.org/10.1080/07373937.2022.2048847 (2022).
6. Fonseca, F., Pénicaud, C., Tymczyszyn, E. E., Gómez-Zavaglia, A. & Passot, S. Factors influencing the membrane fluidity and the impact on production of lactic acid bacteria starters. *Appl Microbiol Biotechnol.* **103**, 6867–6883, https://doi.org/10.1007/s00253-019-10002-1 (2019).
7. Tripathi, M. K. & Giri, S. K. Probiotic functional foods: Survival of probiotics during processing and storage. *J. Funct. Foods* **9**, 225–241, https://doi.org/10.1016/j.jff.2014.04.030 (2014).
8. Han X. et al. Synergizing artificial intelligence and probiotics: A comprehensive review of emerging applications in health promotion and industrial innovation.*Trends Food Sci. Technol.* 104938, https://doi.org/10.1016/j.tifs.2025.104938 (2025).

9. Su, Y. et al. *Lactobacillus paracasei* JY062 alleviates glucolipid metabolism disorders via the adipoinsular axis and gut microbiota. Nutrients. 16, https://doi.org/10.3390/nu16020267 (2024).
10. Ya, T. et al. Immunological evaluation of *Lactobacillus casei* Zhang: a newly isolated strain from koumiss in Inner Mongolia, China. *BMC Immunol.* **9**, 68, https://doi.org/10.1186/1471-2172-9-68 (2008).
11. Wang, Y. et al. Protective effects of probiotic *Lactobacillus casei* Zhang against endotoxin- and d-galactosamine-induced liver injury in rats via anti-oxidative and anti-inflammatory capacities. *Int Immunopharmacol.* **15**, 30–37, https://doi.org/10.1016/j.intimp.2012.10.026 (2013).
12. hang, W. et al. Complete genome sequence of *Lactobacillus casei* Zhang, a new probiotic strain isolated from traditional homemade koumiss in Inner Mongolia, China. *J Bacteriol.* **192**, 5268–5269, https://doi.org/10.1128/jb.00802-10 (2010).
13. Maleknia, M., Ahmadirad, N., Golab, F., Katebi, Y. & Haj Mohamad Ebrahim Ketabforoush, A. DNA methylation in cancer: Epigenetic view of dietary and lifestyle factors.*Epigenet. Insights* **2023**, 25168657231199893, https://doi.org/10.1177/25168657231199893 (2023).
14. Pinho, R. M. & Maga, E. A. DNA methylation as a regulator of intestinal gene expression. *Br. J. Nutr.* **126**, 1611–1625, https://doi.org/10.1017/s0007114521000556 (2021).
15. Moore, L. D., Le, T. & Fan, G. DNA methylation and its basic function. *Neuropsychopharmacology* **38**, 23–38, https://doi.org/10.1038/npp.2012.112 (2013).
16. Adhikari, S. & Curtis, P. D. DNA methyltransferases and epigenetic regulation in bacteria. *FEMS Microbiol. Rev.* **40**, 575–591, https://doi.org/10.1093/femsre/fuw023 (2016).
17. Boulias, K. & Greer, E. L. Means, mechanisms and consequences of adenine methylation in DNA. *Nat. Rev. Genet.* **23**, 411–428, https://doi.org/10.1038/s41576-022-00456-x (2022).
18. Marinus, M. G. & Casadesus, J. Roles of DNA adenine methylation in host-pathogen interactions: Mismatch repair, transcriptional regulation, and more. *FEMS Microbiol. Rev.* **33**, 488–503, https://doi.org/10.1111/j.1574-6976.2008.00159.x (2009).
19. Hui, W. et al. A novel bacteriophage exclusion (BREX) system encoded by the *pglX* gene in *Lactobacillus casei* Zhang. *Appl. Environ. Microbiol.* **85**, e01001–e01019, https://doi.org/10.1128/aem.01001-19 (2019).
20. Zhang, W., Sun, Z., Menghe, B. & Zhang, H. Short communication: Single molecule, real-time sequencing technology revealed species- and strain-specific methylation patterns of 2 *Lactobacillus* strains. *J. Dairy Sci.* **98**, 3020–3024, https://doi.org/10.3168/jds.2014-9272 (2015).
21. Zhao, J. et al. Roles of adenine methylation in the physiology of *Lacticaseibacillus paracasei*. *Nat. Commun.* **14**, 2635, https://doi.org/10.1038/s41467-023-38291-1 (2023).
22. Her, J.-Y., Kim, M. S. & Lee, K.-G. Preparation of probiotic powder by the spray freeze-drying method. *J. Food Eng.* **150**, 70–74, https://doi.org/10.1016/j.jfoodeng.2014.10.029 (2015).
23. Bodzen, A. et al. Design of a new lyoprotectant increasing freeze-dried *Lactobacillus* strain survival to long-term storage. *BMC Biotechnol.* **21**, 66, https://doi.org/10.1186/s12896-021-00726-2 (2021).
24. Yan, J., Wu, M., Kwok, L.-y. & Zhang, W. Adenine DNA methylation is involved in regulating ethanol and osmotic stress responses in *Lacticaseibacillus paracasei* Zhang. *Food Front.* **4**, 1347–1361, https://doi.org/10.1002/fft2.279 (2023).
25. Zhang, M.-Y., Juan, Z., Long, L., Du, G.-C. & Jian, C. Influence of key acid-resistant genes in arginine metabolism on stress tolerance in *Lactococcus lactis* NZ9000. *Microbiol. China* **44**, 314–324, https://doi.org/10.13344/j.microbiol.china.160119 (2017).
26. Chen, Q. & Amster-Choder, O. BglF, the sensor of the bgl system and the beta-glucosides permease of *Escherichia coli*: evidence for dimerization and intersubunit phosphotransfer. *Biochemistry* **37**, 8714–8723, https://doi.org/10.1021/bi9731652 (1998).
27. Brinkkötter, A., Klöss, H., Alpert, C. & Lengeler, J. W. Pathways for the utilization of N-acetyl-galactosamine and galactosamine in *Escherichia coli*. *Mol. Microbiol.* **37**, 125–135, https://doi.org/10.1046/j.1365-2958.2000.01969.x (2000).
28. He, Q. et al. Comparative genomic analysis of *Enterococcus faecalis*: Insights into their environmental adaptations. *BMC Genomics* **19**, 527, https://doi.org/10.1186/s12864-018-4887-3 (2018).
29. Orchard, L. M. & Kornberg, H. L. Sequence similarities between the gene specifying 1-phosphofructokinase (fruK), genes specifying other kinases in *Escherichia coli* K12, and lacC of *Staphylococcus aureus*. *Proc. Biol. Sci.* **242**, 87–90, https://doi.org/10.1098/rspb.1990.0108 (1990).
30. Stolz, B., Huber, M., Marković-Housley, Z. & Erni, B. The mannose transporter of *Escherichia coli*. Structure and function of the IIABMan subunit. *J. Biol. Chem.* **268**, 27094–27099, https://doi.org/10.1016/S0021-9258(19)74222-7 (1993).
31. Sprenger, G. A. Two open reading frames adjacent to the *Escherichia coli* K-12 transketolase (tkt) gene show high similarity to the mannitol phosphotransferase system enzymes from *Escherichia coli* and various gram-positive bacteria. *Biochim. Biophys. Acta* **1158**, 103–106, https://doi.org/10.1016/0304-4165(93)90103-f (1993).
32. Nobelmann, B. & Lengeler, J. W. Molecular analysis of the gat genes from *Escherichia coli* and of their roles in galactitol transport and metabolism. *J. Bacteriol.* **178**, 6790–6795, https://doi.org/10.1128/jb.178.23.6790-6795.1996 (1996).
33. Choi, S. & Kim, E. B. A comprehensive longitudinal study of gut microbiota dynamic changes in laying hens at four growth stages prior to egg production. *Anim. Biosci.* **36**, 1727–1737, https://doi.org/10.5713/ab.23.0271 (2023).
34. Zhang, M. et al. Human breast milk: The role of its microbiota and metabolites in infant health. *J. Agric. Food Chem.* **72**, 10665–10678, https://doi.org/10.1021/acs.jafc.3c07690 (2024).
35. Yang, S. et al. Prevention and treatment of antibiotics-associated adverse effects through the use of probiotics: A review. *J. Adv. Res.* https://doi.org/10.1016/j.jare.2024.06.006 (2024).
36. Andersson, U., Levander, F. & Rådström, P. Trehalose-6-phosphate phosphorylase is part of a novel metabolic pathway for trehalose utilization in *Lactococcus lactis*. *J. Biol. Chem.* **276**, 42707–42713, https://doi.org/10.1074/jbc.M108279200 (2001).
37. Saier, M. H. Jr Bacterial phosphoenolpyruvate: sugar phosphotransferase systems: structural, functional, and evolutionary interrelationships. *Bacteriol. Rev.* **41**, 856–871, https://doi.org/10.1128/br.41.4.856-871.1977 (1977).
38. Efiuvwevwere, B. J. O., Gorris, L. G. M., Smid, E. J. & Kets, E. P. W. Mannitol-enhanced survival of *Lactococcus lactis* subjected to drying. *Appl Microbiol Biotechnol.* **51**, 100–104, https://doi.org/10.1007/s002530051369 (1999).
39. Rambhatla, P., Kumar, S., Floyd, J. T. & Varela, M. F. Molecular cloning and characterization of mannitol-1-phosphate dehydrogenase from *Vibrio cholerae*. *J. Microbiol. Biotechnol.* **21**, 914–920, https://doi.org/10.4014/jmb.1104.04020 (2011).
40. Roux, C., Salmon, L. & Verchère-Béaur, C. Preliminary studies on the inhibition of D-sorbitol-6-phosphate 2-dehydrogenase from *Escherichia coli* with substrate analogues. *J. Enzym. Inhib. Med. Chem.* **21**, 187–192, https://doi.org/10.1080/14756360500535260 (2006).
41. Zuljan, F. A., Repizo, G. D. & Alarcon, S. H. α-Acetolactate synthase of *Lactococcus lactis* contributes to pH homeostasis in acid stress conditions. *Int J. Food Microbiol.* **188**, 99–107, https://doi.org/10.1016/j.ijfoodmicro.2014.07.017 (2014).
42. Nandi, S. & Dey, M. Biochemical and structural insights into how amino acids regulate pyruvate kinase muscle isoform 2. *J. Biol. Chem.* **295**, 5390–5403, https://doi.org/10.1074/jbc.RA120.013030 (2020).

43. Oemcke, L. A., Anderson, R. C., Altermann, E., Roy, N. C. & McNabb, W. C. The role of segmented filamentous bacteria in immune barrier maturation of the small intestine at weaning. *Front. Nutr.* **8**, 759137, https://doi.org/10.3389/fnut.2021.759137 (2021).
44. Matic, J. N. et al. The pyruvate dehydrogenase complex of Mycoplasma hyopneumoniae contains a novel lipoyl domain arrangement. *Gene* **319**, 99–106, https://doi.org/10.1016/s0378-1119(03)00798-4 (2003).
45. Kobayashi, M. A., Watada, H., Kawamori, R. & Maeda, S. Overexpression of acetyl-coenzyme A carboxylase beta increases proinflammatory cytokines in cultured human renal proximal tubular epithelial cells. *Clin. Exp. Nephrol.* **14**, 315–324, https://doi.org/10.1007/s10157-010-0296-x (2010).
46. Lee, S., Jeon, E., Jung, Y. & Lee, J. Heterologous co-expression of accA, fabD, and thioesterase genes for improving long-chain fatty acid production in *Pseudomonas aeruginosa* and *Escherichia coli*. *Appl. Biochem. Biotechnol.* **167**, 24–38, https://doi.org/10.1007/s12010-012-9644-5 (2012).
47. Chaturvedi, S. et al. Overexpression and repression of key rate-limiting enzymes (acetyl CoA carboxylase and HMG reductase) to enhance fatty acid production from *Rhodotorula mucilaginosa*. *J. Basic Microbiol.* **61**, 4–14, https://doi.org/10.1002/jobm.202000407 (2021).
48. Coulibaly, I. et al. The resistance to freeze-drying and to storage was determined as the cellular ability to recover its survival rate and acidification activity. *Int J. Microbiol.* **2010**, 625239, https://doi.org/10.1155/2010/625239 (2010).
49. Hansen, M. L., Petersen, M. A., Risbo, J., Hümmer, M. & Clausen, A. Implications of modifying membrane fatty acid composition on membrane oxidation, integrity, and storage viability of freeze-dried probiotic, *Lactobacillus acidophilus* La-5. *Biotechnol. Prog.* **31**, 799–807. https://doi.org/10.1002/btpr.2074 (2015).
50. Jingjing, E. et al. Effects of buffer salts on the freeze-drying survival rate of *Lactobacillus plantarum* LIP-1 based on transcriptome and proteome analyses. *Food Chem.* **326**, 126849, https://doi.org/10.1016/j.foodchem.2020.126849 (2020).
51. Jingjing, E. et al. Effects of different initial pH values on freeze-drying resistance of *Lactiplantibacillus plantarum* LIP-1 based on transcriptomics and proteomics. *Food Res. Int.* **149**, 110694, https://doi.org/10.1016/j.foodres.2021.110694 (2021).
52. de Carvalho, C. & Caramujo, M. J. The various roles of fatty acids. *Molecules* **23**, 2583, https://doi.org/10.3390/molecules23102583 (2018).
53. Siroli, L. et al. *Lactobacillus paracasei* A13 and high-pressure homogenization stress response. *Microorganisms* **8**, 439, https://doi.org/10.3390/microorganisms8030439 (2020).
54. Heath, R. J. & Rock, C. O. Roles of the FabA and FabZ beta-hydroxyacyl-acyl carrier protein dehydratases in *Escherichia coli* fatty acid biosynthesis. *J. Biol. Chem.* **271**, 27795–27801, https://doi.org/10.1074/jbc.271.44.27795 (1996).
55. Lai, C. Y. & Cronan, J. E. Beta-ketoacyl-acyl carrier protein synthase III (FabH) is essential for bacterial fatty acid synthesis. *J. Biol. Chem.* **278**, 51494–51503, https://doi.org/10.1074/jbc.M308638200 (2003).
56. Yang, X. et al. Transcriptional regulator AcrR increases ethanol tolerance through regulation of fatty acid synthesis in *Lactobacillus plantarum*. *Appl. Environ. Microbiol.* **85**, e01690–19, https://doi.org/10.1128/aem.01690-19 (2019).
57. Wu, C., Huang, J. & Zhou, R. Progress in engineering acid stress resistance of lactic acid bacteria. *Appl. Microbiol. Biotechnol.* **98**, 1055–1063, https://doi.org/10.1007/s00253-013-5435-3 (2014).
58. Brennan, M., Wanismail, B., Johnson, M. C. & Ray, B. Cellular damage in dried *Lactobacillus acidophilus*. *J. Food Prot.* **49**, 47–53, https://doi.org/10.4315/0362-028x-49.1.47 (1986).
59. Castro, H. P., Teixeira, P. M. & Kirby, R. Changes in the cell membrane of *Lactobacillus bulgaricus* during storage following freeze-drying. *Biotechnol. Lett.* **18**, 99–104, https://doi.org/10.1007/BF00137819 (1996).
60. Wang, Y., Delettre, J., Guillot, A., Corrieu, G. & Beal, C. Influence of cooling temperature and duration on cold adaptation of *Lactobacillus acidophilus* RD758. *Cryobiology* **50**, 294–307, https://doi.org/10.1016/j.cryobiol.2005.03.001 (2005).
61. Johnsson, T., Nikkila, P., Toivonen, L., Rosenqvist, H. & Laakso, S. Cellular fatty acid profiles of *lactobacillus* and *lactococcus* strains in relation to the oleic Acid content of the cultivation medium. *Appl. Environ. Microbiol.* **61**, 4497–4499, https://doi.org/10.1128/aem.61.12.4497-4499.1995 (1995).
62. Lonvaud-Funel, A. & Desens, C. Constitution des acides gras des membranes des bactéries lactiques du vin : incidences des conditions de culture. *Sci. Aliments* **10**, 817–829 (1990).
63. Keweloh, H. & Heipieper, H. J. Trans unsaturated fatty acids in bacteria. *Lipids* **31**, 129–137, https://doi.org/10.1007/bf02522611 (1996).
64. Russell, N. J. Mechanisms of thermal adaptation in bacteria: blueprints for survival. *Trends Biochem. Sci.* **9**, 108–112, https://doi.org/10.1016/0968-0004(84)90106-3 (1984).
65. Dong, H. et al. A cryptic long-chain 3-ketoacyl-ACP synthase in the *Pseudomonas putida* F1 unsaturated fatty acid synthesis pathway. *J. Biol. Chem.* **297**, 100920, https://doi.org/10.1016/j.jbc.2021.100920 (2021).
66. Wu, G. Amino acids: metabolism, functions, and nutrition. *Amino Acids* **37**, 1–17, https://doi.org/10.1007/s00726-009-0269-0 (2009).
67. Hoskins, A. A., Anand, R., Ealick, S. E. & Stubbe, J. The formylglycinamide ribonucleotide amidotransferase complex from *Bacillus subtilis*: metabolite-mediated complex formation. *Biochemistry* **43**, 10314–10327, https://doi.org/10.1021/bi049127h (2004).
68. Wang, J. et al. Combined proteomic and transcriptomic analysis of the antimicrobial mechanism of tannic acid against *Staphylococcus aureus*. *Front. Pharm.* **14**, 1178177, https://doi.org/10.3389/fphar.2023.1178177 (2023).
69. De Man, J., Rogosa, M. & Sharpe, M. E. A medium for the cultivation of lactobacilli. *J. Appl. Bacteriol.* **23**, 130–135, https://doi.org/10.1111/J.1365-2672.1960.TB00188.X (1960).
70. Thompson, A. et al. Tandem mass tags: a novel quantification strategy for comparative analysis of complex protein mixtures by MS/MS. *Anal. Chem.* **75**, 1895–1904, https://doi.org/10.1021/ac0262560 (2003).
71. González-Fernández, M. J., Fabrikov, D., Ramos-Bueno, R. P., Guil-Guerrero, J. L. & Ortea, I. SWATH differential abundance proteomics and cellular assays show in vitro anticancer activity of arachidonic acid- and docosahexaenoic acid-based monoacylglycerols in HT-29 colorectal cancer cells. *Nutrients* **11**, 2984, https://doi.org/10.3390/nu11122984 (2019).

Acknowledgements

This research was supported by the National Natural Science Foundation of China (Grant No. 32372304), the Program for Innovative Research Team in Universities of Inner Mongolia Autonomous Region (NMGIRT2411), the Inner Mongolia Autonomous Region Science and Technology Leading Talent Team Project (2022LJRC0003), and the Central Guiding Local Science and Technology Development Fund Project (2024ZY0168).

Author contributions

Wenyi Zhang: Conceptualization, Supervision, Project administration, Funding acquisition, Review. Hui Qiao and Mingkun You: Writing-Conceptualization, Methodology, Formal analysis, Writing-original draft. Jiaming Yan: Methodology, Validation, Visualization. Meng Zhang: Data curation. Lai-Yu Kwok: Writing—Review & Editing. All authors read and approved the final manuscript.

Competing interests
The authors declare no competing interests.

Additional information
Supplementary information The online version contains supplementary material available at https://doi.org/10.1038/s41538-025-00409-8.

Correspondence and requests for materials should be addressed to Wenyi Zhang.